Desalination and Water Treatment
www.deswater.com
doi: 10.5004/dwt.2020.24831

174 (2020) 279–290
January

Preparation of sodium-substituted xonotlite from eggshell and its adsorption behavior for cadmium(II)

Wenqing Tang[a,b], Youzhi Dai[a,c,*], Rongying Zeng[b,*], Biao Gu[b], Zhimin Zhang[b], Huiyan He[b]

[a]*School of Chemical Engineering, Xiangtan University, Xiangtan, Hunan 411105, China, emails: daiyzh@xtu.edu.cn (Y. Dai), wqtang518@163.com (W. Tang)*
[b]*Key Laboratory of Functional Organometallic Materials of College of Hunan Province, College of Chemistry and Material Science, Hengyang Normal University, Hengyang 421008, People's Republic of China, China, emails: zengry13@163.com (R. Zeng), biaogu@hynu.edu.cn (B. Gu), 2570035061@qq.com (Z. Zhang), 1491056418@qq.com (H. He)*
[c]*College of Environmental and Resources, Xiangtan University, Xiangtan, Hunan 411105, China*

Received 15 February 2019; Accepted 23 August 2019

ABSTRACT

Sodium-substituted xonotlite (NaCSH) was prepared from eggshell by using hydrothermal method and doping technology, and was used to remove cadmium(II) from aqueous solution. NaCSH had porous structure and large surface area as characterized by BET surface area, scanning electron microscopy (SEM) and energy dispersive spectroscopy (EDX). Batch adsorption experiments showed that the removal efficiency and adsorption capacity came to 98.01% and 98.01 mg/g, respectively, at pH 6.0, temperature 313 K and contact time of 45 min. Further analysis revealed that cadmium(II) adsorption onto $NaCSH_2$ was best described by Langmuir isotherm model ($R^2 > 0.988$), and kinetics data were best fitted by pseudo-second order kinetics ($R^2 > 0.99$). The calculated maximum adsorption capacity of cadmium(II) on $NaCSH_2$ was 150.07 mg/g at 313 K, which is much higher than pure xonotlite. Thermodynamic studies revealed that the adsorption process was spontaneous and endothermic. Moreover, $NaCSH_2$ was found to retain greater adsorption capacity for cadmium(II) after five cycles of adsorption–desorption. Thus, $NaCSH_2$ may be a good adsorbent to remove cadmium(II) from wastewater.

Keywords: Waste eggshell; Synthetic; $NaCSH_2$; Cadmium(II); Adsorption; Regeneration

1. Introduction

In recent years, with the rapid industrialization and technological advance, heavy metals are universally regarded as a threat toward human health and our environment [1,2]. The primary source leading to water pollution is due to the industrial wastewater from electroplating [3], pigment [4], plastic [5], etc. Removal of these pollutants from wastewater has been continuously studied through a range of strategies such as chemical reduction, electrodialysis, ion exchange and adsorption [6–9]. Among these methods, adsorption is one of the most effective, practical and economical methods owing to its high adsorption efficiency, simple design and strong operability for metal ions [10]. Recently, various environment-friendly materials have been used for the adsorption of heavy metal ions, such as minerals materials (zeolites, kaolinite, bentonite, hydrotalcite, sepiolite) [11–15], polymers [16], biomaterials [17], activated carbon [18,19]. To develop cheap and highly efficient adsorption materials, however, more studies are required.

Xonotlite ($Ca_6(Si_6O_{17})(OH)_2$) is one of hydrous calcium silicate hydrates (CSH), and mainly occur in nature as hydrothermal alteration products found in serpentine or

* Corresponding authors.

contact zone of metamorphic rock [20]. It has been widely used in building lightweight and thermal insulation materials due to its good thermal stability [21,22]. To improve its functional properties, some investigators introduced Mg^{2+}, Co^{2+}, Ni^{2+} and other ions by doping technology to replace calcium ions of xonotlite [23,24]. A study found that a certain amount of metal ions contribute to the formation of xonotlite [25]. Notably, xonotlite has also been considered as a kind of adsorbent under good development as it can be easily obtained at low cost and can be easily synthesized [26]. Specifically, xonotlite can remove organic pollutants such as humic and fulvic [26] and inorganic pollutants such as phosphate [27]. However, there are few studies on the adsorption of heavy metals on xonotlite of doping alkali metal ion.

In this study, we attempt to develop an efficient removal method of the heavy metal ion by the adsorption on xonotlite of doping alkali metal ion. Sodium-substituted xonotlite (NaCSH) with porous structure and large surface area was prepared by the sonochemical method assisted hydrothermal synthesis. NaCSH was prepared by introducing sodium ions to replace part of calcium ions in the process of synthesized artificial xonotlite and used to remove cadmium(II) from aqueous solution. The effect of pH, initial cadmium(II) concentration, contact time and temperature on CSH and NaCSH was investigated. The adsorption capacity and mechanism of the two adsorbents were compared.

2. Materials and methods

2.1. Chemicals and reagents

All the chemicals and reagents used in the experiments were of analytical grade. Stock solution (1,000 ± 3 mg/L) of Cd(II) ions was prepared by $Cd(CH_3CO_2)_2$ (AR, J&K Scientific Ltd., China). Fresh dilutions were used in each experiment. The deionized water was produced by Milli-Q system.

2.2. Preparation of CSH and NaCSH

Eggshell (Hengyang city, Hunan province, China) was cleaned, dried and crushed into eggshell particle. CaO powder was prepared by baking eggshell particle at 850°C for 4 h in muffle furnace. After cooling to room temperature, the powder above was sieved to yield 200 mesh CaO. Then 50.0 g CaO and 100 mL deionized water were put into a 250-mL beaker, which were stirred for 30 min, aged for 5 h to make colloidal $Ca(OH)_2$.

Colloidal $Ca(OH)_2$ and SiO_2 with Ca/Si molar ratio1:1 were added to deionized water in 250-mL conical flask with continuous ultrasound application at 50°C–60°C (suspension solution A), and adding four different proportion sodium chloride to suspension solution A with Na/(Ca + Na) molar ratio 0.5:6, 1:6, 2:6 and 3:6. Then, the mixture was pretreated using ultrasonic wave for 60 min and transferred into autoclave reactor for hydrothermal growth for 9 h at 230°C. After standing for 24 h, four NaCSH samples ($NaCSH_1$, $NaCSH_2$, $NaCSH_3$ and $NaCSH_4$) were obtained. The precipitate was filtered and washed with 0.1 mol/L HCl aqueous solution, deionized water and ethanol. After dried at 70°C, the solid was ground and sifted to yield 200 mesh products. Pure xonotlite sample (CSH) was prepared without adding sodium chloride. The reactions were described in the following chemical Eqs. (1) and (2).

$$Ca(OH)_2 + SiO_2 + Na^+ + H_2O \rightarrow Na_xCa_{6-2x}(Si_6O_{17})(OH)_2 \quad (1)$$

$$Ca(OH)_2 + SiO_2 + H_2O \rightarrow Ca_6(Si_6O_{17})(OH)_2 \quad (2)$$

2.3. Characterization of CSH and NaCSH

2.3.1. Analytical method

The specific surface area of $NaCSH_1$, $NaCSH_2$, $NaCSH_3$ and $NaCSH_4$ was determined by BET technique. Average pore diameter and pore volume of the samples were measured with a Micromeritics ASAP 2010 Device (Micromeritics, USA).

NaCSH with the highest specific surface area ($NaCSH_2$) and CSH were characterized using X-ray diffraction (XRD, Rigaku MiniFlex X-ray diffractometer, Japan). Scanning electron microscopy with energy spectrum (SEM–EDX) was conducted with a Merlin compact SEM (Carl Zeiss, Germany) to observe the surface microstructures and constituent elements of the samples.

2.3.2. Solubility experiments of $NaCSH_2$

The release of Ca^{2+} from $NaCSH_2$ was investigated by a sequences of batch experiments. For each experiment, 1 g of CSH and $NaCSH_2$ was mixed with 1 L of deionized water in glass bottle. Then, the bottles were stirred for 5, 10, 20, 30, 40, 50 and 60 min at 313 K. The resulting Ca^{2+} concentration was determined using the EDTA coordination titration method [28]. Solution pH was tested by pH330i-meter.

The release of Ca^{2+} increased with the increase of reaction time in the range of 0–40 min, while the concentration of Ca^{2+} release changed little from 40 to 60 min (Fig. 1). Concentration of Ca^{2+} release is 1.18 mg/L at 40 min (Fig. 1). The amount of Ca^{2+} released from $NaCSH_2$ is so small that it cannot cause the ascension of water hardness. This may be due to eggshell containing a small amount of magnesium [29]. Previous studies have found that magnesium silicate hydrates persisted even after 1 year, the silica concentrations remained at 1–2 mM [30].

2.4. Point of zero charge (pH_{PZC})

The pH value was tested by pH330i-meter (WTW corporation, Germany). The point of zero charge (pH_{PZC}) is defined as the pH at which the total surface charges become zero, pH_{PZC} for $NaCSH_2$ and CSH were estimated as described previously [31]. The studies were executed in 10 conical flasks with glass stopper which contain 50 mL of 0.01 M $NaNO_3$ solution. The initial pH (pH_i) in the range of 1.0–10.0 was adjusted by 0.1 M NaOH or 0.1 M HNO_3 solutions in each conical flask. 0.12 g CSH or $NaCSH_2$ was added to each conical flask, which were kept for 48 h with intermittent manual shaking to attain the equilibrium. The pH_{PZC} was calculated by the plot of $\Delta(pH_i - pH_f)$ against pH_i, where pH_i and pH_f represent the initial and final pH values, respectively. The pH_{PZC} value was equal to the point of intersection

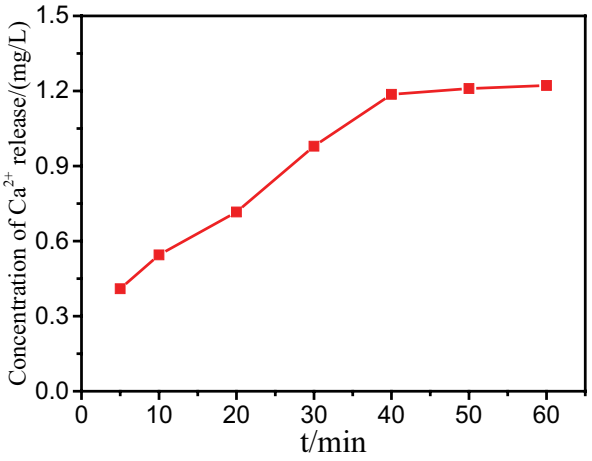

Fig. 1. Concentration of Ca^{2+} released from $NaCSH_2$.

of the resulting curve with abscissa. The pH_{PZC} for CSH and $NaCSH_2$ were determined to be 6.02 and 5.42, respectively.

2.5. Batch adsorption experiments

To obtain the optimum Cd(II) adsorption conditions by $NaCSH_2$ and CSH, the batch adsorption studies were performed to determine the optimum pH, initial Cd(II) concentration, contact time and temperature. The experiments were performed by the amount of $NaCSH_2$ or CSH in 100 mL of Cd(II) ion solution in 250 mL conical flasks and shaking for 45 min at different temperature (293, 303 and 313 K) at 250 rpm. The residual concentration of Cd(II) ion was determined using the flame atomic absorption spectrophotometer (FAAS) (PE700, PE Company, USA). Each experiment was performed in triplicate and the average value was used in this study. Removal rate (ϱ,%) and adsorption capacity of Cd(II) ion on the adsorbent was calculated by the following Eqs. (3)–(5), respectively.

$$\rho = \frac{\left(C_0 - C_e\right)}{C_0} \times 100\% \tag{3}$$

$$Q_e = \frac{\left(C_0 - C_e\right)V}{m} \tag{4}$$

$$Q_t = \frac{\left(C_0 - C_t\right)V}{m} \tag{5}$$

where C_0 and C_e (mg/L) are the initial and the equilibrium concentrations of Cd(II) in solution, respectively; Q_e (mg/g) is adsorption quantity of Cd(II) ion on the adsorbent at the time of equilibrium, and Q_t (mg/g) was the adsorption capacity at time t; V (L) is volume of solution and m (g) is mass of adsorbent.

2.6. Adsorption isotherm

The adsorption isotherm is an effective method to evaluate adsorption behavior on adsorbent at the same temperature. Presently, the common adsorption isotherms are Langmuir model, Freundlich model, Dubinin–Radushkevich model and Temkin model [32–34], which are given by Eqs. (6)–(11):

Langmuir model:

$$Q_e = \frac{\left(K_L C_e Q_m\right)}{\left(1 + K_L C_e\right)} \tag{6}$$

Adsorption equilibrium constant R_L equation

$$R_L = \frac{1}{\left(1 + K_L C_0\right)} \tag{7}$$

Freundlich model:

$$\log Q_e = \frac{\log C_e}{n} + \log K_F \tag{8}$$

Dubinin–Radushkevich model (D–R):

$$\ln Q_e = \ln Q_m - K_{DR}\varepsilon^2 \tag{9}$$

$$\varepsilon = RT\ln\left(1 + \frac{1}{C_e}\right) \tag{10}$$

Temkin model:

$$Q_e = \frac{RT\ \ln A}{B} + \frac{RT\ \ln C_e}{B} \tag{11}$$

where Q_m (mg/g) is maximum adsorption capacity; K_L (L/mg) is Langmuir isotherm constant; K_F (g/mg) is Freundlich isotherm constant; K_{D-R} (mol^2/kJ^2) is Dubinin–Radushkevich isotherm constant; R_L is adsorption equilibrium constant, the R_L value indicates whether the adsorption process is irreversible (R_L = 0), favorable (0 < R_L < 1), linear (R_L = 1) or unfavorable (R_L > 1); n are Freundlich constants related to adsorption intensity; ε (mg/L) is adsorptive potential of Polanyi; A (J/mol) is equilibrium binding constant; B (J/mol) is the adsorption strength; R is the ideal gas constant (8.314×10^{-3} kJ/(mol K)); T (K) is the absolute temperature.

2.7. Adsorption kinetics

To further investigate the adsorption process of $NaCSH_2$ and CSH for Cd(II) ion by adsorption kinetic models, four widely applied kinetic models (the Lagergren pseudo-first-order-model, the Lagergren pseudo-second-order-model, the Elovich model and the internal particle diffusion [IPD] model) were applied to analyze the adsorption experimental data [35,36], which are given by Eqs. (12)–(15):

$$\log\left(Q_e - Q_t\right) = \log Q_e - \frac{K_1 t}{2.303} \tag{12}$$

$$\frac{t}{Q_t} = \left(K_2 Q_e^2\right)^{-1} + \frac{t}{Q_e} \tag{13}$$

$$Q_t = \frac{\ln(\alpha\beta)}{\beta} + \frac{\ln t}{\beta} \quad (14)$$

$$Q_t = K_d t^{0.5} + C \quad (15)$$

where Q_t (mg/g) is the adsorption capacity at time t; K_1 (min^{-1}) is the Lagergren pseudo-first-order adsorption rate constant; K_2 (g/[mg min]) is the Lagergren pseudo-second-order adsorption rate constant; α(mg/[g min]) is the initial adsorption rate; β (g/mg) is the desorption constant; K_d (mg·[g min]$^{1/2}$) is the internal diffusion rate constant; C (mg/g) is the constant of the influence of boundary layer thickness at the adsorption process.

2.8. Thermodynamic study

As for thermodynamic study, the sorption parameters including the Gibbs free energy change ($\Delta G°$) and the enthalpy change ($\Delta H°$) and the entropy change ($\Delta S°$) were obtained from the Langmuir equilibrium constant (K_L) (Table 2) variation with temperature (T) by employing non-linear method wherein the values of K_L were first made dimensionless. Thermodynamic parameters were obtained through Eqs. (16)–(18) [33,37,38]:

$$\Delta G° = -RT \ln K_L \quad (16)$$

$$\Delta G° = \Delta H° - T\Delta S° \quad (17)$$

The well-known Van't Hoff equation is obtained by substituting Eq. (17) into Eq. (16)

$$\ln K_L = \frac{\Delta S°}{R} - \frac{\Delta H°}{(RT)} \quad (18)$$

where the Gibbs free energy change ($\Delta G°$) was directly calculated from Eq. (16), while two other thermodynamic parameters ($\Delta H°$ and $\Delta S°$) for adsorption of Cd(II) ion on adsorbent (CSH and $NaCSH_2$) at different temperatures (293, 303 and 313 K) were determined from the slope and intercept of a plot of $\ln K_L$ against $1/T$.

2.9. Regeneration studies

Under optimal adsorption conditions, the adsorption of Cd(II) ion on CSH and $NaCSH_2$ were carried out, then supernatant was filtrated and got adsorbents containing Cd(II) ion. The adsorbents containing Cd(II) ion were desorbed for 4 h at 50 mL of 1% HNO_3 or 1% HCl. The desorbed adsorbents (CSH and $NaCSH_2$) are reused to adsorb Cd(II) ion from aqueous solution with the same experiment methods. The adsorption–desorption experiments were repeated five times in same order. The removal rate of Cd(II) ion on adsorbents (CSH and $NaCSH_2$) were calculated at adsorption equilibrium.

3. Results and discussion

3.1. Characterization of adsorbent

The structural parameters (BET specific surface area, average pore diameter and pore volume) of eggshell powder, CSH, $NaCSH_1$, $NaCSH_2$, $NaCSH_3$, $NaCSH_4$ and $NaCSH_5$ are given in Table 1 (CSH, $NaCSH_1$~$NaCSH_4$: xonotlite and Na-xonotlite were prepared from eggshell powder; $NaCSH_5$: Na-xonotlite was prepared from commercial Cao reagent). The surface area of Na-xonotlite ($NaCSH_1$, $NaCSH_2$, $NaCSH_3$ and $NaCSH_4$) is larger than xonotlite (CSH). Specific surface area of eggshell powder was 10.03 m^2/g; BET of CSH was 98.48 m^2/g; BET of four Na-xonotlite from eggshell powder was greater than 114 m^2/g, yet one of the highest BET of Na-xonotlite from eggshell powder was 126.58 m^2/g; BET of $NaCSH_5$ from commercial Cao reagent was 111.27 m^2/g (Table 1). The results showed that doping sodium ion into xonotlite using eggshell powder was beneficial to increase its S_{BET} and improve its internal pore structure. The reason my be that eggshell contain a small amount of magnesium [29].

Specific surface area (126.58 m^2/g), average pore diameter (6.12 nm) and pore volume (0.51 cm^3/g) of $NaCSH_2$ are the largest among the four Na-xonotlite. However, the structural parameters of Na-xonotlite could not gradually increase with increasing sodium ions content. The possible reason was that the number of doping sodium ions was limited after the replaced calcium ions of xonotlite reached saturation [39]. Thus, $NaCSH_2$ was chosen for removal of Cd(II) ions.

SEM showed that the CSH and $NaCSH_2$ have a fine granular surface and honeycomb-like structure including a lot of pores (Figs. 2a and b). The two adsorbents have high porosity and relatively big specific surface area, indicating that the materials present good characteristics to be employed as an adsorbent for metal ion uptake. A comparison between the SEM of CSH and $NaCSH_2$ revealed that the $NaCSH_2$ had better dispersion and larger pore diameter. Thus, $NaCSH_2$ may have more active adsorption sites than the CSH. TEM images of (a) CaO for eggshell, (b) $NaCSH_2$ for eggshell, (c) $NaCSH_2$ for commercial CaO. $NaCSH_2$ for eggshell (b) and $NaCSH_2$

Table 1
Pore structural parameters of CSH and NaCSH

Sample	Egg shell	CSH	$NaCSH_1$	$NaCSH_2$	$NaCSH_3$	$NaCSH_4$	$NaCSH_5$
S_{BET} (m^2/g)	10.03	98.48	114.83	126.58	123.74	118.67	111.27
D_a (nm)	3.82	5.91	5.87	6.12	6.08	5.99	5.76
V_t (cm^3/g)	0.0091	0.47	0.45	0.51	0.49	0.46	0.44

S_{BET}: BET surface area; D_a: average pore diameter; V_t: total pore volume calculated as the amount of nitrogen adsorbed; CSH, $NaCSH_1$~$NaCSH_4$: xonotlite and Na-xonotlite were prepared from eggshell powder; $NaCSH_5$: Na-xonotlite was prepared from commercial CaO reagent.

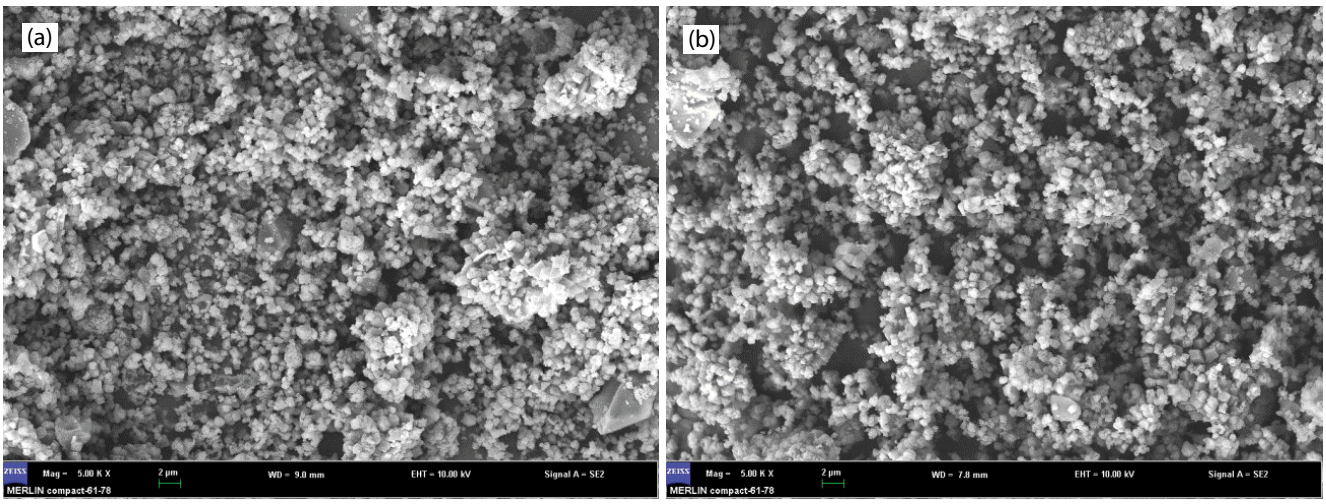

Fig. 2. SEM images of (a) CSH and (b) $NaCSH_2$.

for commercial CaO (c) on surface both have the similar stripe structure (Fig. 3).

The EDX analysis showed that the main components of the synthesized CSH and $NaCSH_2$ were Ca, Si and O elements, and $NaCSH_2$ also contained a small amount of Na element (Fig. 4). The crystal structures of CSH and $NaCSH_2$ were analyzed by XRD (Fig. 5). The diffraction peaks of CSH at around $2\theta = 21°$, 27°, 29° and 32° were indexed (401), (202), (320) and (321) facet, respectively, which were in basic agreement with the standard diffraction pattern of xonotlite (JCPDS Card No.23-0125) [40]. Along with the increasing incorporation of Na^+ ions, the same peak positions and a reduction in peak intensities were observed in comparison with CSH (Fig. 3).

3.2. Effect of pH on Cd(II) removal by $NaCSH_2$ and CSH

The pH of the aqueous solution had an important effect on the adsorptive uptake of Cd(II) ions that it affects speciation of heavy ions and surface properties of sorbent [41]. At pH = 1–14, the distribution coefficient of Cd(II) was analyzed by Visual MINTEQ 3.0. The cadmium species include Cd(II), $Cd_2(OH)^{3+}$, $Cd(OH)^+$, $Cd(OH)_2$, $Cd_2(OH)^{3-}$ and $Cd_2(OH)_4^{2-}$ more than 99.98% of cadmium existed as Cd(II) at a pH value not greater than 6 (Fig. 6). Cd(II) content reduced slightly from 99.98% to 98.36% and the positively charged $Cd_2(OH)^{3+}$ and $Cd(OH)^+$ gradually increased at pH 6.0–8.0. At pH range 8.0–9.0, Cd(II) content reduced to 86.84% and the $Cd_2(OH)^{3+}$, $Cd(OH)^+$and $Cd(OH)_2$ content were gradually increased. At pH 9.0–12.0, Cd(II) content declined sharply from 86.84% to zero, $Cd(OH)_2$ content tend to achieve rapid enhancement from 0.12% to 91.85% in first and then gradually declined. When pH > 12, the total content of $Cd_2(OH)^{3-}$ and $Cd_2(OH)_4^{2-}$ exceeded 98%, while $Cd(OH)_2$ content was less than 1.92%. Therefore, the optimal adsorption pH range was selected at 3.0–7.5.

The influence of aqueous solution pH on Cd(II) uptake by CSH and $NaCSH_2$ is shown in Fig. 7. At low pH (i.e., 3.0) the removal efficiency was about 52% and 70% for CSH and $NaCSH_2$, respectively. In the range of pH 3.0–5.5, the removal rate of cadmium ions on CSH and $NaCSH_2$ increased sharply with the increasing pH value of the solution; When $5.5 < pH \leq 7.0$, the removal rate on CSH was first gradually increased, and then the removal rate on $NaCSH_2$ was stable. Similar results were obtained when cadmium ions were adsorbed by magnetized and nonmagnetized

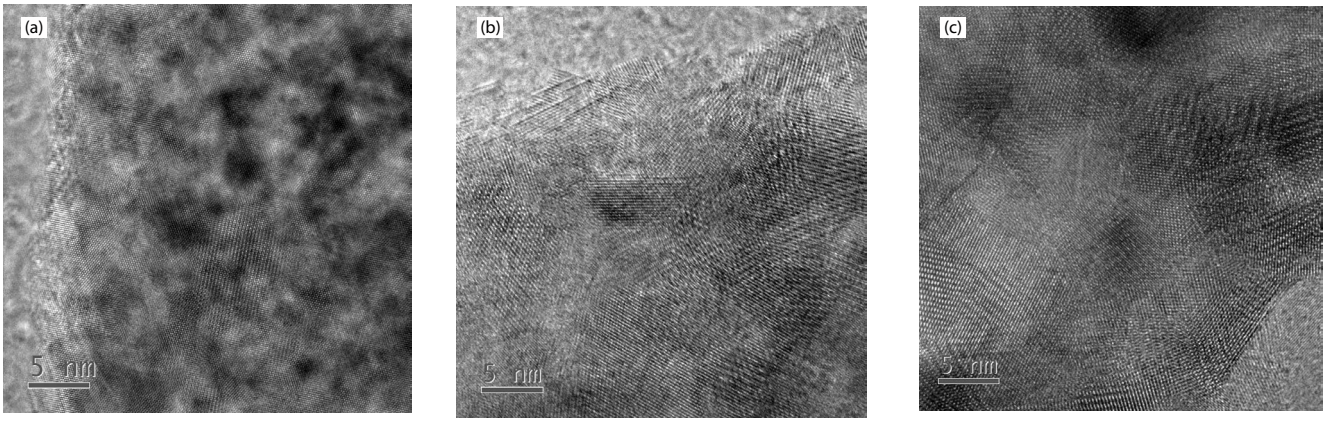

Fig. 3. TEM images of (a) CaO for eggshell, (b) $NaCSH_2$ for eggshell, (c) $NaCSH_2$ for commercial CaO.

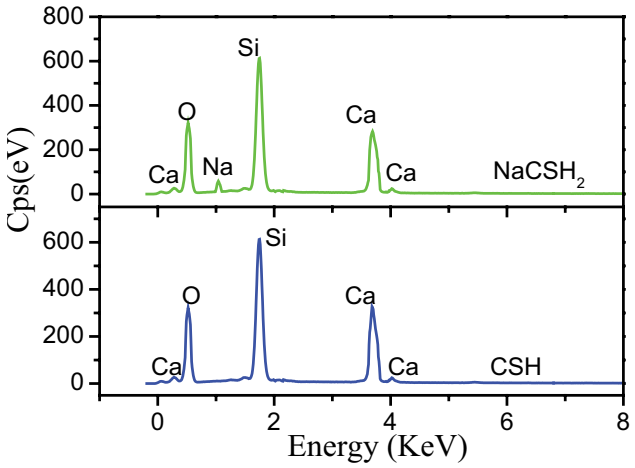

Fig. 4. EDX of CSH and $NaCSH_2$.

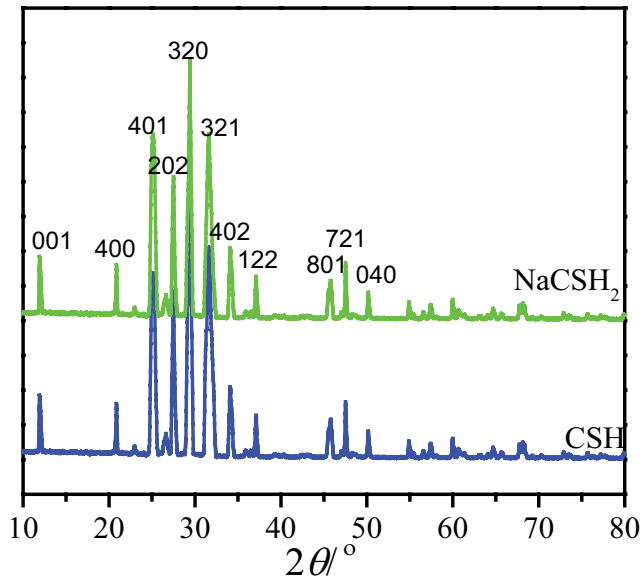

Fig. 5. XRD pattern of CSH and $NaCSH_2$.

biochar in earlier literature [42].The possible reason is that H^+ (or H_3O^+) and Cd^{2+} ions competed for the adsorption sites on the CSH and $NaCSH_2$. At lower pH values (pH < pH_{PZC}, pH_{PZC} for CSH and $NaCSH_2$ were 6.02 and 5.42, respectively), and H^+ (or H_3O^+) ions are able to quickly occupied the surface adsorption sites at CSH and $NaCSH_2$ from the Cd^{2+} ions adsorption process that the CSH and $NaCSH_2$ were highly positively charged surface (Ca–OH_2^+ may be the dominant elements) and hence there is a repulsion between the positively charged surface and Cd^{2+} ions. At high pH values (pH > pH_{PZC}, ≡Si-O^- may be the dominant elements), only less H^+ (or H_3O^+) ions compete against Cd^{2+} ions for bonding sites, as Cd^{2+} ions can easily contact with the free adsorption sites [43,44]; on the other hand, the negative charge on the adsorbent's surface form static adsorption with the positive charge of cadmium ion (see Fig. 4, Cd^{2+} content in excess of 98%, and a few $Cd_2(OH)^{3+}$ and $Cd(OH)^+$ at pH ≤ 7.0) and augment adsorption. This argument is very well supported

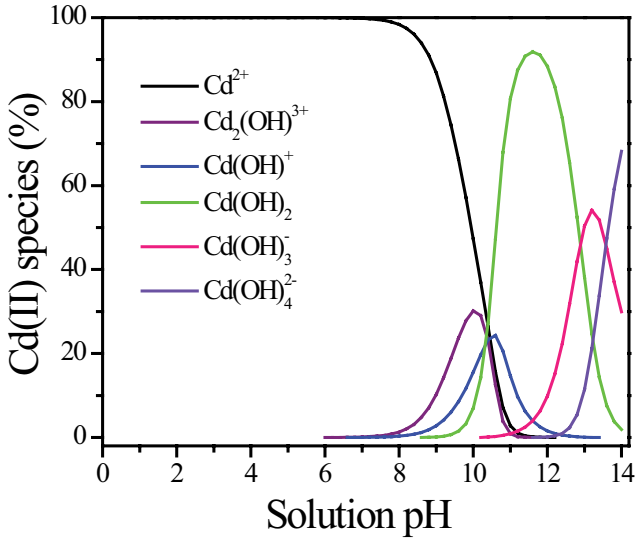

Fig. 6. Chemical speciation of cadmium ions with different pH in water.

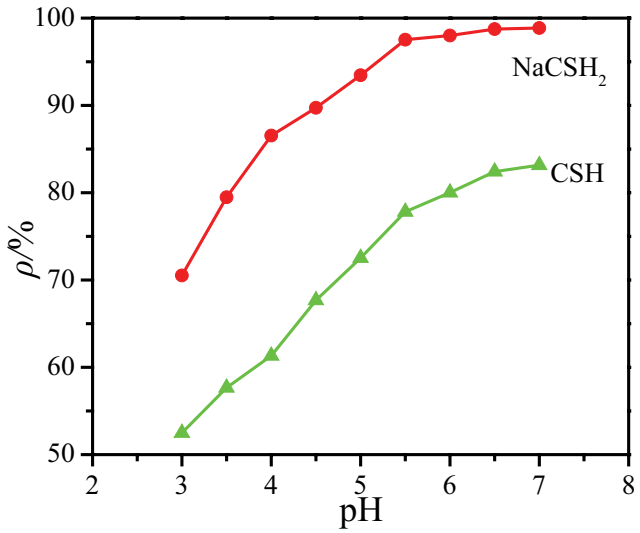

Fig. 7. Effect of the adsorption of Cd^{2+} on CSH or $NaCSH_2$.

by zero point charge studies. Some studies have shown that Ca–OH and Si–OH bonds were present in the calcium silicate hydrate [45,46] and Pb(II) or Nd(III) can exchange Ca^{2+} in the calcium silicate hydrate [47]. The ions are adsorbed on the adsorbent surface and then diffuses into the voids of the C–S–H, which can combine the heavy metal ions with the hydroxyl groups on the surface by a strong chemical adsorption [48,49]. Thus, there may be strong chemical adsorption between cadmium ions and CSH or $NaCSH_2$.

$$\equiv Si-O^- + Cd^{2+} \rightarrow \equiv Si-OCd^+ \quad (19)$$

Therefore, pH 6.0 was chosen as the optimal pH at which the high removal rate of Cd^{2+} ions on CSH and $NaCSH_2$ was emerged.

3.3. Effect of adsorbent dosage

The effect of adsorbent dosage was studied in the range of 0.3–1.8 g/L and is plotted in Fig. 8. It shows that increasing CSH and $NaCSH_2$ dosage increased the removal rate (from 52.48% to 83.15% for CSH, and 70.52% to 98.86% for $NaCSH_2$), and the removal rate of Cd(II) on $NaCSH_2$ was significantly higher than that of CSH. The removal rate of Cd(II) on $NaCSH_2$ and CSH came to the peak (98.01% and 81.68%, respectively) at 1.2 g/L of the adsorbent dosage and could be regarded as the basic adsorption equilibrium. When the adsorbent dosage was continuing to increase the removal rate of $NaCSH_2$ and CSH has risen by only just about 2.42% and 0.80%, respectively. Therefore, 1.2 g/L of the adsorbent dosage was used in other adsorption experiments.

3.4. Effect of initial concentration at different temperatures

The adsorption experiments for Cd(II) in aqueous solution on $NaCSH_2$ and CSH were observed at 30–180 mg/L of initial Cd(II) concentration and various temperatures (293, 303 and 313 K). As seen from Fig. 9, although the removal rates of Cd(II) declined with increasing of initial Cd(II) concentration at three temperatures, the removal rate of CSH decreased more than $NaCSH_2$. The adsorption of Cd(II) on $NaCSH_2$ still could keep high removal rate (93.98%, 95.95% and 98.01%, respectively) at a 120 mg/L of the initial Cd^{2+} concentration at 293, 303 and 313 k. The highest removal rate of $NaCSH_2$ was obtained at 313 K. Therefore, the initial Cd(II) concentration and reaction temperature were chosen for 120 mg/L and 313 K, respectively.

3.5. Effect of contact time

The effect of different contact time on the adsorption of Cd(II) by $NaCSH_2$ and CSH is shown in Fig. 8. The removal rates of Cd(II) on $NaCSH_2$ and CSH rapidly increased with the increase of contact time in the range of 0–45 min, while the removal rate changed little from 45 to 180 min (Fig. 10).

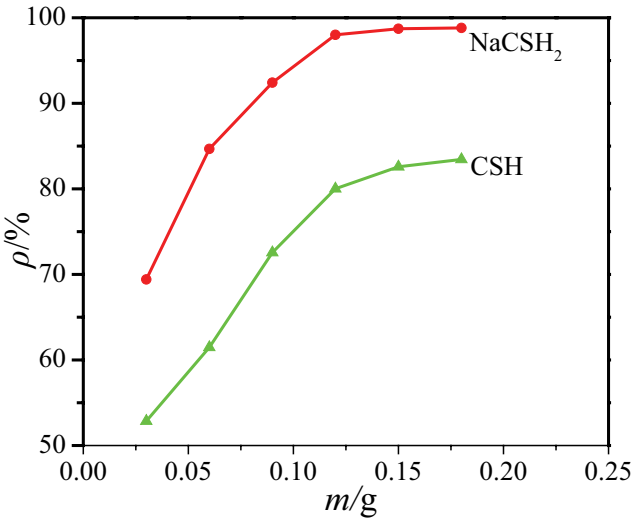

Fig. 8. Effect of CSH and $NaCSH_2$ dosage on the adsorption of Cd^{2+}.

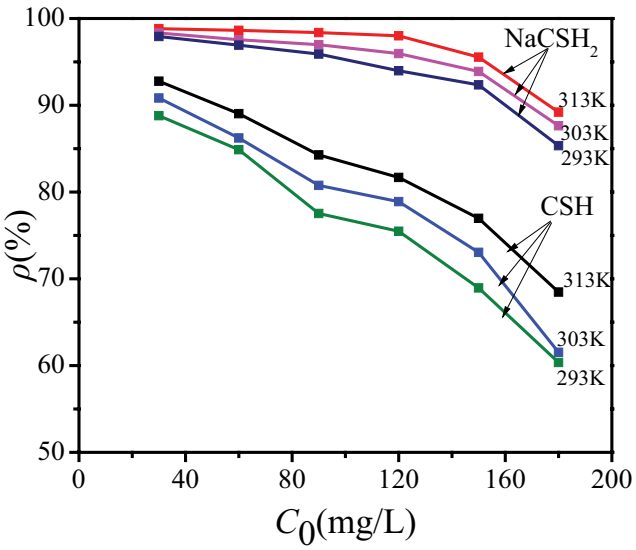

Fig. 9. Effect of initial Cd^{2+} concentration on removal rate.

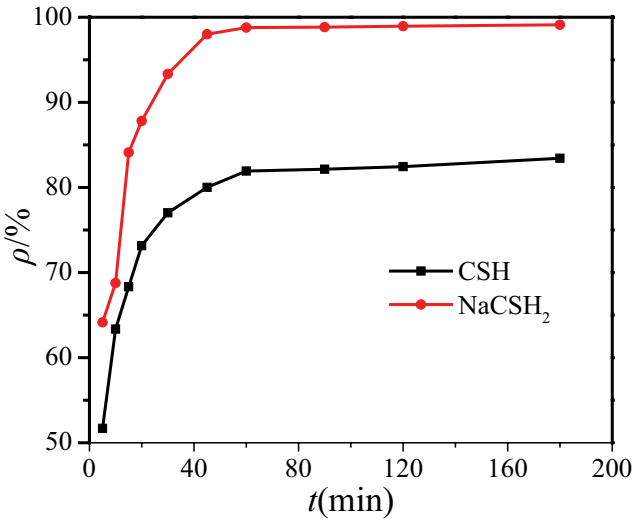

Fig. 10. Effect of contact time on the adsorption of Cd^{2+} on removal rate.

Notably, the removal rate of Cd(II) on the $NaCSH_2$ (98.01%) was significantly higher than that of CSH (80.01%). Thus, the contact time 45 min was enough for reaching adsorption equilibrium of Cd(II) on $NaCSH_2$ and CSH.

3.6. Elution and recycle

After adsorbing heavy metal ions, the adsorbent would be recycled and reused by successful elution to obtain the maximum economic benefits, which is an important factor for measuring the economic and environment protection aspects of an adsorbent [50,51]. $NaCSH_2$ and CSH were eluted efficiently with 1% HCl or 1% HNO_3. The adsorption and desorption were continuously repeated for five times (Fig. 11). From the first to the fifth cycle, the removal rates of Cd(II) on $NaCSH_2$ and CSH was decreased 8.25%

(HNO_3 elution) and 10.18% (HCl elution), 9.10% (HNO_3 elution), 11.07% (HCl elution), respectively. $NaCSH_2$ still could keep higher removal rate (87.27% or 82.46%) in the fifth cycle for adsorption of Cd(II), suggesting it is a good adsorbent.

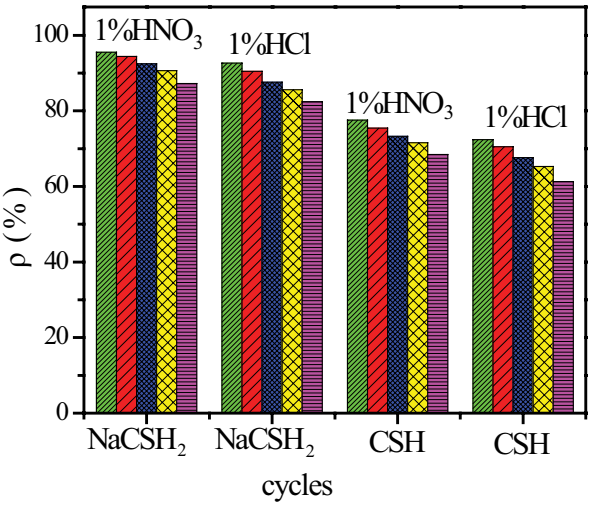

Fig. 11. Regeneration experiment.

3.7. Adsorption isotherm

The adsorption isotherm constants of Cd(II) on $NaCSH_2$ and CSH at 293, 303 and 313 K are shown in Table 2. The equilibrium data of $NaCSH_2$ followed the following order to fit isotherms: Langmuir (R^2: 0.9885–0.9931) > Temkin (R^2: 0.9567–0.9850) > D–R (R^2: 0.8948–0.9745) > Freundlich (R^2: 0.8569–0.9540); However, the equilibrium data of CSH followed: D–R (R^2: 0.9838–0.9889) > Langmuir (R^2: 0.9791–0.9873) > Temkin (R^2: 0.9661–0.9827) > Freundlich (R^2: 0.9570–0.9772). The results showed that the R^2 of the Langmuir model for $NaCSH_2$ ($R^2 > 0.988$) were the higher than those of other three models; the R^2 of the D–R model for CSH ($R^2 > 0.983$) were the higher than other three models, but the R^2 of the Langmuir model is near the R^2 of the D–R model. The correlation coefficient are comprehensively considered for adsorption of Cd(II) on $NaCSH_2$ and CSH, suggesting that Langmuir model was suitable for describing the adsorption characteristics of Cd(II) on $NaCSH_2$ and CSH. Furthermore, the maximum adsorption capacity (Q_m) from Langmuir model increased with increasing temperature, indicating that the increasing temperature was conducive to the adsorption reaction in adsorption process. This is contrasted with other materials reported by some literatures in Table 3. Although the Q_m of $NaCSH_2$

Table 2
Isotherm model parameters for adsorption of Cd(II) onto $NaCSH_2$ and CSH at different temperature

Isotherm models	Sample	Parameters	293 K	303 K	313 K
Langmuir	$NaCSH_2$	Q_m (mg g^{-1})	146.98	149.29	150.07
		K_L (L g^{-1})	0.2487	0.35455	0.6969
		R^2	0.9931	0.9979	0.9885
		R_L	0.022–0.118	0.015–0.086	0.008–0.046
	CSH	Q_m (mg g^{-1})	110.90	116.55	125.85
		K_L (L g^{-1})	0.0664	0.0764	0.0825
		R^2	0.9833	0.9791	0.9873
		R_L	0.077–0.334	0.068–0.304	0.063–0.2877
Freundlich	$NaCSH_2$	K_F (mg g^{-1})	35.15	40.07	51.87
		$1/n$	0.45	0.45	0.41
		R^2	0.9540	0.9354	0.8569
	CSH	K_F (mg g^{-1})	14.06	15.67	17.42
		$1/n$	0.47	0.46	0.47
		R^2	0.9708	0.9570	0.9772
D–R	$NaCSH_2$	Q_m (mg g^{-1})	707.72	443.75	726.22
		K_{D-R} (mol^2 kJ^{-1})	0.0033	0.0028	0.0029
		R^2	0.9745	0.9264	0.8948
	CSH	Q_m (mg g^{-1})	413.33	431.58	494.36
		K_{D-R} (mol^2 kJ^{-1})	0.0039	0.0038	0.0038
		R^2	0.9838	0.9739	0.9889
Temkin	$NaCSH_2$	A (mg L^{-1})	377.75	474.76	950.59
		B (J mol^{-1})	88.49	86.30	92.19
		R^2	0.9850	0.9821	0.9567
	CSH	A (mg L^{-1})	80.80	99.09	111.51
		B (J mol^{-1})	111.37	109.65	100.75
		R^2	0.9827	0.9661	0.9826

Table 3
Comparison of the maximum adsorption capacity of Cd(II) ion by various adsorbents

Adsorbents	Initial heavy metal Concentration (mg/L)	Q_m (mg/g)	References
MBC	10–250	–11 (318 K)	[42]
PAC	50–1,000	104.17 (303 K)	[52]
CAC	50–1,000	90.09 (303 K)	[52]
SCAC	50–1,000	126.58 (303 K)	[52]
SPAC	50–1,000	142.86 (303 K)	[52]
Iron oxide modified clay-activated carbon composite beads	10–300	41.3 (298 K)	[53]
Mesoporous activated carbon	20–200	227.27 (298 K)	[54]
MCS-SH		601.51 (293 K)	[55]
MCS		436.14 (293 K)	[55]
Mesoporous silica	4.6–47.6	3.619 (298 K)	[56]
CSH	30–180	110.90 (293 K)	This work
		116.55 (303 K)	
		125.85 (313 K)	
$NaCSH_2$	30–180	146.98 (293 K)	
		149.29 (303 K)	
		150.07 (313 K)	

MBC: Magnetic biochar was produced by magnetite (Fe_3O_4) precipitation onto Douglas fir biochar, PAC: prepared activated carbon from nut shells, CAC: commercial activated carbon, SCAC: sulfurized commercial activated carbon, SPAC: sulfurized prepared activated carbon from nut shells, MCS-SH: thiol-functionalized mesoporous calcium silicate, MCS: unmodified mesoporous calcium silicate.

was lower than that of mesoporous activated carbon, thiol-functionalized mesoporous calcium silicate (MCS-SH) and unmodified mesoporous calcium silicate (MCS), it was higher than that of commercial activated carbon, those of the modified activated carbon and mesoporous silica. Of note, the adsorption of Cd(II) ion on $NaCSH_2$ has greater adsorption capacity than CSH.

Adsorption equilibrium constants (R_L) calculated according to the Langmuir isotherm constant (K_L) directly reflected to the difficulty and easy degree of the adsorption process [32], which were all less than 1, suggesting that the adsorption of Cd(II) in the solution on $NaCSH_2$ and CSH were very easy and showed strong adsorption ability. The Freundlich isotherm constant $\left(\frac{1}{n}\right)$ was less than 1, which also indicated that $NaCSH_2$ and CSH were preferential adsorbent for Cd(II) [33]. The equilibrium binding constant (A) of Temkin adsorption model became larger with increase of reaction temperature, suggesting that the adsorption ability of Cd(II) in the solution on CSH and $NaCSH_2$ increased with the increase of temperature.

3.8. Adsorption kinetics

The experimental data were computed with four adsorption kinetic models, and the correlation parameters and equilibrium adsorption capacity of the experimental values ($Q_{e,\exp}$) are listed in Table 4. The results showed that the pseudo-second order kinetic model had the highest correlation coefficient ($R^2 > 0.99$), and the calculated theoretical adsorption capacity ($Q_{e,\text{cal}}$) is very close to the experimental data ($Q_{e,\exp}$), suggesting that the pseudo-second order kinetic model was suitable to describe the adsorption kinetics of Cd(II) ion on $NaCSH_2$ and CSH.

The slope and intercept of the Elovich kinetic model reflect the adsorption rate and adsorption capacity of the adsorbate, respectively [57]. According to the initial adsorption rate of Elovich model, increasing the adsorption temperature is beneficial to speed up the initial adsorption rate of Cd(II) ion on $NaCSH_2$ and CSH. The intercepts ($C > 0$) of the fitting IPD model does not pass through the coordinate origin, indicating that the ion internal diffusion is not the only control step of adsorption rate [58]. It can be inferred that the adsorption of Cd(II) ion on $NaCSH_2$ and CSH would include comprehensive control process of multiple actions such as external liquid film diffusion, surface adsorption and particle internal diffusion.

3.9. Thermodynamic study

The Gibbs free energy change (ΔG^0) was directly calculated from Eq. (16), while two other thermodynamic parameters (ΔH^0 and ΔS^0) for the adsorption of Cd(II) ion on adsorbent ($NaCSH_2$ and CSH) at different temperatures (293, 303 and 313 K) were determined from the slope and intercept of a plot of $\ln K_L$ against $1/T$ (Fig. 12). The linear fitting equations are $y = -5{,}152.0x + 27.698$ ($R^2 = 0.9372$) for $NaCSH_2$ and $y = -1{,}088.5x + 12.625$ ($R^2 = 0.9421$) for CSH, respectively. The values of three thermodynamic parameters (ΔG^0, ΔH^0 and ΔS^0) are shown in Table 5. The values of ΔG^0 are negative and decreased with the increase of the temperature, which revealed that the adsorption is spontaneous. The positive value of ΔH^0 showed that the adsorption for Cd(II) ion on adsorbent ($NaCSH_2$ and CSH) was an endothermic process [59], suggesting that physical adsorption may be the main factor in this adsorption process. The positive value of ΔS^0 for Cd(II) ion on adsorbent ($NaCSH_2$ and CSH) indicated that

Table 4
Kinetic model parameters for adsorption of Cd(II) onto NaCSH and CSH at different temperature

Kinetic models	Sample	Parameters	293 K	303 K	313 K
	$NaCSH_2$	$Q_{e,exp}$ (mg g^{-1})	93.98	95.95	98.01
	CSH	$Q_{e,exp}$ (mg g^{-1})	75.48	78.90	80.10
Pseudo-first-order-model	$NaCSH_2$	$Q_{e,cal}$ (mg g^{-1})	28.85	25.87	25.15
		K_1 (min^{-1})	0.0151	0.0179	0.0216
		R^2	0.9189	0.9111	0.8870
	CSH	$Q_{e,cal}$ (mg g^{-1})	34.04	23.78	20.57
		K_1 (min^{-1})	0.0159	0.0148	0.0304
		R^2	0.9748	0.9291	0.8716
Pseudo-second-order-model	$NaCSH_2$	$Q_{e,cal}$ (mg g^{-1})	100.00	101.01	102.04
		K_2 (g mg^{-1} min^{-1})	0.0026	0.0030	0.0032
		R^2	0.9935	0.9922	0.9948
	CSH	$Q_{e,cal}$ (mg g^{-1})	81.30	83.33	85.47
		K_2 (g mg^{-1} min^{-1})	0.0031	0.0033	0.0035
		R^2	0.9916	0.9914	0.9960
Elovich model	$NaCSH_2$	A (mg g^{-1} min^{-1})	5.968 × 109	3.081 × 1011	4.119 × 1012
		β (g mg^{-1})	6.270	7.138	7.686
		R^2	0.8863	0.8764	0.8664
	CSH	α (mg g^{-1} min^{-1})	3.496 × 108	4.451 × 109	1.067 × 1011
		β (g mg^{-1})	5.983	6.452	7.169
		R^2	0.9241	0.9009	0.8749
IPD model	$NaCSH_2$	K_d (mg $g^{-0.5}$ $min^{-0.5}$)	4.026	3.650	3.474
		C (mg g^{-1})	64.73	64.73	68.22
		R^2	0.7619	0.7413	0.7226
	CSH	K_d (mg $g^{-0.5}$ $min^{-0.5}$)	3.579	3.360	3.073
		C (mg g^{-1})	46.75	50.98	54.88
		R^2	0.8313	0.7859	0.7448

$Q_{e,exp}$: the equilibrium adsorption capacity in the experiment, mg/g; $Q_{e,cal}$: the equilibrium adsorption capacity was calculated by the fitting model, mg/g.

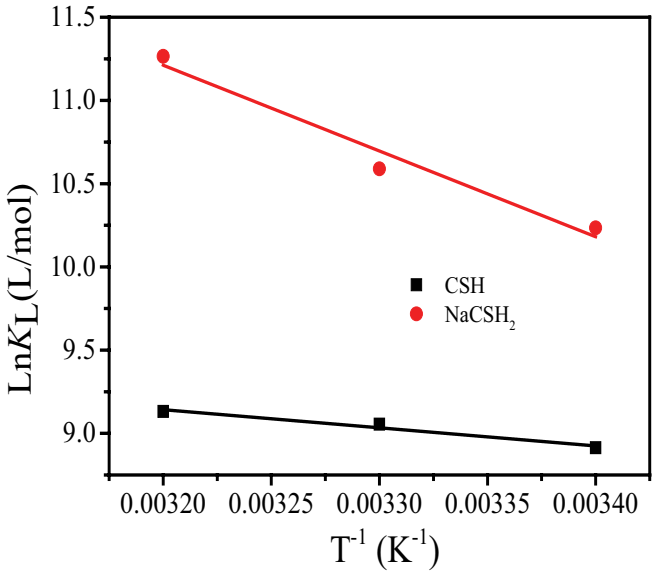

Fig. 12. Relationship curve of lnK_L vs. T^{-1}.

the change of entropy is an important driving force in the adsorption process [15].

3.10. Cost effectiveness of NaCSH

The synthesis process of NaCSH is less cost effective and fast reaction time. The main material for synthesis of NaCSH is eggshell, which is a cheapest material in China. Comparatively, the preparation of single phase gyrolite requires CaO by calcined calcium carbonate from POCH (Poland) at 1,000°C for 2 h, and it has been successfully synthesized under hydrothermal conditions at 200°C for 24 h within the CaO–SiO_2–Na_2O–H_2O system [60]. The response time of single phase gyrolite is 2.6 times higher than that of NaCSH. Moreover, the maximum adsorption of Cd^{2+} on the NaCSH (149.29 mg/g at 303 K) was higher to commercial activated carbon (CAC) (90.09 mg/g at 303 K) [52]. Thus, NaCSH is a low cost and environmentally green material.

4. Conclusion

The adsorption function materials ($NaCSH_2$ and CSH) with well-developed microscopic pore structure were

Table 5
Thermodynamic parameters for sorption of Cd(II) onto $NaCSH_2$ and CSH

Adsorbent	T (K)	$\Delta G°$ (kJ mol^{-1})	$\Delta H°$ (kJ mol^{-1})	$\Delta S°$ (J mol^{-1} K^{-1})
$NaCSH_2$	293	–24.64	42.83	230.28
	303	–26.94		
	313	–29.24		
CSH	293	–21.70	9.05	104.96
	303	–22.75		
	313	–23.80		

synthesized using eggshell. $NaCSH_2$ and CSH are good adsorbents to remove Cd(II) ion from aqueous solution as they had large adsorption capacity, high adsorption efficiency, convenient operation and regeneration. $NaCSH_2$ had higher adsorption capacity than raw CSH. Specifically, the maximum adsorption efficiency (81.68% for CSH, and 98.01% for $NaCSH_2$) and equilibrium adsorption capacity (81.68 mg/g for CSH, and 98.01 mg/g for $NaCSH_2$) after 45 min at 313 K, pH 6 and initial Cd(II) concentration of 120 mg/L. Langmuir isotherms with high correlation coefficient at 293, 303 and 313 K were more suitable for describing the adsorption behavior. The kinetics of the adsorption for Cd(II) ion on $NaCSH_2$ and CSH were found to fit the pseudo-first-order-model. The thermodynamic parameters of the adsorption indicated that the adsorption of Cd(II) ion on $NaCSH_2$ and CSH were a spontaneous and endothermic process, and the adsorption was enhanced by the increase of temperature. These results suggested that the main adsorption mechanism of Cd(II) ion on $NaCSH_2$ and CSH may involve physical adsorption.

Compared with other materials in the adsorption of Cd(II), $NaCSH_2$ and CSH exhibited better adsorption performance. The low adsorption coverage ratio of $NaCSH_2$ and CSH for Cd(II) showed that the material still has considerable potential to be improved to get higher adsorption capacity. Altogether, our results showed that $NaCSH_2$ could be a good adsorbent to remove heavy metals from wastewater.

Acknowledgments

This study is supported by the Hunan Provincial Science and Technology Plan Project (No. 2018SK2021), Key Laboratory of Functional Organometallic Materials of Hunan Province College (No. GN18K02, No. GN19K06); National Training Program of Innovation and Entrepreneurship for Undergraduate (No. CX1814) and College students' research learning and innovative experimental program of Hunan Province (No. cx1814, No. 2018255773, No. S201910546024, No. S201910546002X).

References

[1] S.O. Lesmana, N. Febriana, F.E. Soetaredjo, J. Sunarso, S. Ismadji, Studies on potential applications of biomass for the separation of heavy metals from water and wastewater, J. Biochem. Eng., 44 (2009) 19–41.
[2] I. Ali, P. Damdimopoulou, U. Stenius, A. Adamsson, S.I. Mäkelä, A. Åkesson, M. Berglund, H. Håkansson, K. Halldin, Cadmium-induced effects on cellular signaling pathways in the liver of transgenic estrogen reporter mice, Toxicol. Sci., 127 (2012) 66–75.
[3] Y.G. Zhou, N.V. Rees, R.G. Compton, Nanoparticle-electrode collision processes: the electroplating of bulk cadmium on impacting silver nanoparticles, Chem. Phys. Lett., 511 (2011) 183–186.
[4] F. Rosi, C. Grazia, F. Gabrieli, A. Romani, M. Paolantoni, R. Vivani, B.G. Brunetti, P. Colomban, C. Miliani, UV–Vis-NIR and micro Raman spectroscopies for the non destructive identification of Cd1-xZnxSsolid solutions in cadmium yellow pigments, Microchem. J., 124 (2016) 856–867.
[5] S.M. Jin, M.J. Burek, N.D. Evans, Z. Jahed, T.Y. Tsui, Fabrication and plastic deformation of sub-micron cadmium structures, Scripta Mater., 66 (2012) 619–622.
[6] B.B. Li, X.Y. Jin, J.J. Lin, Z.L. Chen, Green reduction of graphene oxide by sugarcane bagasse extract and its application for the removal of cadmium in aqueous solution, J. Cleaner Prod., 189 (2018) 128–134.
[7] L. Marder, A.M. Bernardes, J.Z. Ferreira, Cadmium electroplating wastewater treatment using a laboratory-scale electrodialysis system, Sep. Purif. Technol., 37 (2004) 247–255.
[8] S. Edebali, E. Pehlivan, Evaluation of chelate and cation exchange resins to remove copper ions, Powder Technol., 301 (2016) 520–525.
[9] R.Y. Zeng, W.Q. Tang, X. Liu, C.X. Ding, D.X. Gong, Adsorption of Cu2+from aqueous solutions by Si-substituted carbonate hydroxyapatite prepared from egg-shell: kinetics, isotherms and mechanism studies, Desal. Wat. Treat., 116 (2018) 137–147.
[10] G.L. Huang, D. Wang, S.L. Ma, J.L. Chen, L. Jiang, P.Y. Wang, A new, low-cost adsorbent: preparation, characterization, and adsorption behavior of Pb(II) and Cu(II), J. Colloid Interface Sci., 445 (2015) 294–302.
[11] J.M. Hua, Adsorption of low-concentration arsenic from water by co-modified bentonite with manganese oxides and poly(dimethyldiallylammonium chloride), J. Environ. Chem. Eng., 6 (2018) 156–168.
[12] Q.L. Qiu, X.G. Jiang, G.J. Lv, Z.L. Chen, S.Y. Lu, M.J. Ni, J.H. Yan, X.B. Deng, Adsorption of heavy metal ions using zeolite materials of municipal solid waste incineration fly ash modified by microwave-assisted hydrothermal treatment, Powder Technol., 335 (2018) 156–163.
[13] G. Zhou, Z.M. Jiang, S.Q. Wei, A new hydrotalcite-like absorbent FeMnMg-LDH and its adsorption capacity for Pb^{2+} ions in water, Appl. Clay Sci., 153 (2018) 29–37.
[14] J.Y. Huang, Z.W. Wu, L.W. Chen, Y.B. Sun, The sorption of Cd(II) and U(VI) on sepiolite: a combined experimental and modeling studies, J. Mol. Liq., 209 (2015) 706–712.
[15] M.W. Amer, A.M. Awwad, Removal of As(V) from aqueous solution by adsorption onto nanocrystalline kaolinite: equilibrium and thermodynamic aspects of adsorption, Environ. Nanotechnol. Monit. Manage., 9 (2018) 37–41.
[16] J.Y. He, Y.L. Li, C.M. Wang, K.S. Zhang, D.Y. Lin, L.T. Kong, J.H. Liu, Rapid adsorption of Pb, Cu and Cd from aqueous solutions by β-cyclodextrin polymers, Appl. Surf. Sci., 426 (2017) 29–39.
[17] Z.Z. Li, T. Katsumi, S. Imaizumi, X.W. Tang, T. Inui, Cd(II) adsorption on various adsorbents obtained from charred biomaterials, J. Hazard. Mater., 183 (2010) 410–420.
[18] R. Lelifajri, R. Nurfatimah, Preparation of polyethylene glycol diglycidyl ether (PEDGE) crosslinked chitosan/activated carbon

composite film for Cd^{2+} removal, Carbohydr. Polym., 199 (2018) 499–505.
[19] H.C. Ge, J.C. Wang, Ear-like poly (acrylic acid)-activated carbon nanocomposite: a highly efficient adsorbent for removal of Cd(II) from aqueous solutions, Chemosphere, 169 (2017) 443–449.
[20] P. Mandaliev, E. Wieland, R. Dähn, J. Tits, S.V. Churakov, O. Zaharko, Mechanisms of Nd(III) uptake by 11Å tobermorite and xonotlite, Appl. Geochem., 25 (2010) 763–777.
[21] Y. Konuklu, O. Ersoy, Fabrication and characterization of form-stable phase change material/xonotlite microcomposites, Sol. Energy Mater. Sol. Cells, 168 (2017) 130–135.
[22] G.S. Wei, X.X. Zhang, F. Yu, Thermal conductivity measurements on xonotlite-type calcium silicate by the transient hot-strip method, J. Univ. Sci. Technol. Beijing, Mineral Metallurgy Material, 15 (2008) 791–795.
[23] S. Komarmeni, R. Roy, D.M. Roy, Pseudomorphism in xonotlite and tobermorite with Co^{2+} and Ni^{2+} exchange for Ca^{2+} at 25°C, Cem. Concr. Res., 16 (1986) 47–58.
[24] O.P. Shrivastava, S. Komarnenit, E. Breval, Mg^{2+} uptake by synthetic tobermorite and xonotlite, Cem. Concr. Res., 21 (1991) 83–90.
[25] W. Nocun-Wczelik, Effect of some inorganic admixtures on the formation and properties of calcium silicate hydrates produced in hydrothermal conditions, Cem. Concr. Res, 27 (1997) 83–92.
[26] H. Katsumata, S. Kaneco, R. Matsuno, K. Itoh, K. Masuyama, T. Suzuki, K. Funasaka, K. Ohta, Removal of organic poly-electrolytes and their metal complexes by adsorption onto xonotlite, Chemosphere, 52 (2003) 99–915.
[27] X. Chen, H. Kong, D. Wu, X. Wang, Y. Lin, Phosphate removal and recovery through crystallization of hydroxyapatite using xonotlite as seed crystal, J. Environ. Sci., 21 (2009) 575–580.
[28] W. Guan, F. Ji, D. Fang, Y. Cheng, Z. Fang, Q. Chen, P. Yan, Porosity formation and enhanced solubility of calcium silicate hydrate in hydrothermal synthesis, Ceram. Int., 40 (2014) 1667–1674.
[29] K. Prabakaran, A. Balamurugan, S. Rajeswari, Development of calcium phosphate based apatite from hen's eggshell, Bull. Mater. Sci., 28 (2005) 115–119.
[30] D. Nied, K. Enemark-Rasmussen, E. L'Hopital, J. Skibsted, B. Lotenbach, Properties of magnesium silicate hydrates (M-S-H), Cem. Concr. Res., 79 (2016) 323–332.
[31] M. Ghasemi, M. Naushad, N. Ghasemi, Y. Khosravi-fard, Adsorption of Pb(II) from aqueous solution using new adsorbents prepared from agricultural waste: adsorption isotherm and kinetic studies, J. Ind. Eng. Chem., 20 (2014) 2193–2199.
[32] S.G. Chen, R.T. Yang, Theoretical basis for the potential theory adsorption isotherms. The Dubinin-Radushkevich and Dubinin-Astakhov equations, Langmuir, 10 (1994) 4244–4249.
[33] A. Waheed, M. Mansha, I.W. Kazi, N. Ullah, Synthesis of a novel 3,5-diacrylamidobenzoic acid based hyper-cross-linked resin for the efficient adsorption of Congo Red and Rhodamine B, J. Hazard. Mater., 369 (2019) 528–538.
[34] W.Q. Tang, R.Y. Zeng, Y.L. Feng, X.M. Li, W. Zhen, Removal of Cr(VI) from aqueous solution by nano-carbonate hydroxylapatite of different Ca/P molar ratios, Chem. Eng. J., 223 (2013) 340-346.
[35] P. Pal, S.S. Syed, F. Banat, Gelatin-bentonite composite as reusable adsorbent for the removal of lead from aqueous solutions: Kinetic and equilibrium studies, J. Water Process Eng., 20 (2017) 40–50.
[36] Z.H. Wang, D.K. Shen, F. Shen, C.F. Wu, S. Gu, Equilibrium, kinetics and thermodynamics of cadmium ions (Cd^{2+}) removal from aqueous solution using earthworm manure-derived carbon materials, J. Mol. Liq., 241 (2017) 612–621.
[37] K. Agathian, L. Kannammal, B. Meenarathi, S. Kailash, R. Anbarasan, Synthesis, characterization and adsorption behavior of cotton fiber based Schiff base, Int. J. Biol. Macromol., 107 (2018) 1102–1112.
[38] R.Y. Zeng, W.Q. Tang, X. Liu, C.X. Ding, D.X. Gong, Adsorption of Zn^{2+} from aqueous solutions by Si-substituted carbonate hydroxyapatite: equilibrium, kinetics, and mechanism, Environ. Prog. Sustain., 37 (2018) 2073–2081.
[39] G.R. Qian, G.L. Xu, H.Y. Li, A.M. Li, Mg-xonotlite and its coexisting phases, Cem. Concr. Res., 27 (1997) 315–320.
[40] J.J. Zou, C.B. Guo, Y.S. Jiang, C.D. Wei, F.F. Li, Structure, morphology and mechanism research on synthesizing xonotlite fiber from acid-extracting residues of coal fly ash and carbide slag, Mater. Chem. Phys., 172 (2016) 121–128.
[41] S.L. Wan, J.Y. Wu, S.S. Zhou, R. Wang, B. Gao, F. He, Enhanced lead and cadmium removal using biochar-supported hydrated manganese oxide (HMO) nanoparticles: behavior and mechanism, Sci. Total Environ., 616–617 (2018) 1298–1306.
[42] A.G. Karunanayake, O.A. Todd, M. Crowley, L. Ricchetti, C.U. Pittman Jr, R. Anderson, D. Mohan, T. Mlsna, Lead and cadmium remediation using magnetized and nonmagnetized biochar from Douglas fir, Chem. Eng. J., 331 (2018) 480–491.
[43] T.A. Salah, A.M. Mohammad, M.A. Hassan, B.E. El-Anadouli, Development of nano-hydroxyapatite/ chitosan composite for cadmium ions removal in wastewater treatment, J. Taiwan Inst. Chem. Eng., 45 (2014) 1571–1577.
[44] G.Y. Tian, W.B. Wang, L. Zong, A.Q. Wang, MgO/palygorskite adsorbent derived from natural Mg-rich brine and palygorskite for high-efficient removal of Cd(II) and Zn(II) ions, J. Environ. Chem. Eng., 5 (2017) 1027–1036.
[45] X. Cong, R. Kirkpatrick, ^{29}Si and ^{17}O NMR investigation of the structure of some crystalline calcium silicate hydrates, Advn. Cem. Bas. Mat. 3 (1996) 133–143.
[46] D. Hou, Z. Lu, T. Zhao, Q. Ding, Reactive molecular simulation on the ordered crystal and disordered glass of the calcium silicate hydrate gel, Ceram. Int., 42 (2016) 4333–4346.
[47] D. Lee, Formation of leadhillite and calcium lead silicate hydrate (C-Pb-S-H) in the solidification/ stabilization of lead contaminants, Chemosphere, 66 (2007)1727–1733.
[48] R. Zak, J. Deja, Spectroscopy study of Zn, Cd, Pb and Cr ions immobilization on C-S-H phase, Spectrochim. Acta A, 134 (2015) 614–620.
[49] Z. Zhang, X. Wang, H. Wang, J, Zhao, Removal of Pb(II) from aqueous solution using hydroxyapatite/calcium silicate hydrate (HAP/C-S-H) composite adsorbent prepared by a phosphate recovery process, Chem. Eng. J., 344 (2018) 53–61.
[50] M.R. Awual, M.M. Hasan, A novel fine-tuning mesoporous adsorbent for simultaneous lead(II) detection and removal from wastewater, Sensor Actuat B-Chem., 202 (2014) 395–403.
[51] M.R. Awual, New type mesoporous conjugate material for selective optical copper(II) ions monitoring and removal from polluted waters, Chem. Eng. J., 307 (2017) 85–94.
[52] A. F. Tajar, T. Kaghazchi, M. Soleimani, Adsorption of cadmium from aqueous solutions on sulfurized activated carbon prepared from nut shells, J. Hazard. Mater., 165 (2009) 1159–1164.
[53] R. R. Pawar, Lalhmunsiama, M. Kim, J.-G. Kim, S.-M. Hong, Efficient removal of hazardous lead, cadmium, and arsenic from aqueous environment by iron oxide modified clay-activated carbon composite beads, Appl. Clay Sci., 162 (2018) 339–350.
[54] I.A.W. Tan, J.C. Chan, B.H. Hameed, L.L.P. Lim, Adsorption behavior of cadmium ions onto phosphoric acid-impregnated microwave-induced mesoporous activated carbon, J. Water Process Eng., 14 (2016) 60–70.
[55] L. Liu, T. Li, G. Yang, Y. Wang, A. Tang, Y. Ling, Synthesis of thiol-functionalized mesoporous calcium silicate and its adsorption characteristics for heavy metal ions, J. Environ. Chem. Eng., 5 (2017) 6201–6215.
[56] Lalchhingpuii, D. Tiwari, Lalhmunsiama, S.M. Lee, Chitosan templated synthesis of mesoporous silica and its application in the treatment of aqueous solutions contaminated with cadmium(II) and lead(II), Chem. Eng. J., 328 (2017) 434–444.
[57] H.N. Tran, C.C. Lin, S.H. Woo, H.P. Chao, Efficient removal of copper and lead by Mg/Al layered double hydroxides intercalated with organic acid anions: adsorption kinetics, isotherms, and thermodynamics, Appl. Clay Sci., 154 (2018) 17–27.
[58] T.S. Yan, X.G. Luo, X.Y. Lin, J.Y. Yang, Preparation, characterization and adsorption properties for lead (II) of alkali-activated porous leather particles, Colloids Surf. A, 512 (2017) 7–16.
[59] J. Liu, Y.W. Li, G. Wang, C.Y. He, Adsorption of Cr(VI) from aqueous solution by modified waste newspaper fiber, China Environ. Sci., 35 (2015) 1368–1374.
[60] A. Różycka, Ł. Kotwican, J. Małolepszy, Synthesis of single phase gyrolite in the CaO-quartz- Na_2O-H_2O system, Mater. Lett., 120 (2014) 166–169.